TECHNICAL ARTICLE

Tilting of semi-rigid GaF_6 octahedra in GaF_3 at high pressures

Jens-Erik Jørgensen,[1,a] Yaroslav Filinchuk,[2] and Vladimir Dmitriev[3]
[1]*Department of Chemistry, Aarhus University, Aarhus C, Denmark*
[2]*Institute of Condensed Matter and Nanosciences, Universiteé Catholique de Louvain, Place L. Pasteur 1, B-1348, Louvain-la-Neuve, Belgium*
[3]*Swiss-Norwegian Beam Lines, European Synchrotron Radiation Facilities, BP 220, F-38043 Grenoble Cedex, France*

(Received 15 September 2016; accepted 1 December 2016)

The VF_3-type compound GaF_3 has been studied by high-pressure angle-dispersive X-ray diffraction in the pressure range from 0.0001 to 10 GPa. The compression mechanism was found to be highly anisotropic. The *c*-axis shows little pressure dependence (≈0.4%), but exhibits negative linear compressibility up to ≈3 GPa where it achieves its maximum length. In contrast, the length of the *a*-axis is reduced by ≈8.8% at the highest measured pressure and an anomalous reduction in the linear compressibility is observed at 4 GPa. The zero pressure bulk modulus B_0 was determined to $B_0 = 28(1)$ GPa. The compression mechanism of GaF_3 is discussed in terms of deformation of an 8/3/*c*2 sphere-packing model. The volume reduction of GaF_3 is mainly achieved through coupled rotations of the GaF_6 octahedra within the entire measured pressure range, which reduces the volume of the cubooctahedral voids. In addition, the volume of the GaF_6 octahedra also decreases for $p \lesssim 4.0$ GPa, but remains constant above this pressure. The volume reduction of the GaF_6 octahedra is accompanied by an increasing octahedral strain. Isosurfaces of the procrystal electron density are used for visualization of the cubooctahedral voids at different pressures. © *2017 International Centre for Diffraction Data*. [doi:10.1017/S0885715616000701]

Key words: high-pressure, compression mechanism, void space

I. INTRODUCTION

Many metal triflourides, MF_3 including GaF_3, crystallize in the VF_3-type structure (Leblanc *et al.*, 1985; Roos and Meyer, 2001). The VF_3 structure is composed of corner sharing MF_6 octahedra and therefore is structurally related to perovskite-type compounds AMX_3 as well as to the ReO_3 structure (Meisel, 1932). The non-distorted perovskite-type compounds are cubic with space group $Pm\bar{3}m$, while the VF_3 structure, which is derived from the ReO_3 structure by coupled rotations of the MF_6 octahedra around one of the cubic body diagonals, is rhombohedral with space group is $R\bar{3}c$, which is a subgroup of $Pm\bar{3}m$. Structural changes of VF_3-type compounds are conveniently described as a rhombohedral deformation of a sphere packing of type 8/3/*c*2 (Sowa and Ahsbahs, 1998). The spheres of the 8/3/*c*2 sphere packing form octahedral and cubooctahedral voids, and each sphere has eight nearest-neighbour contacts and the smallest mesh has three edges (Fischer, 1973). The volume of the octahedral voids remains constant during a rhombohedral deformation of the 8/3/*c*2 sphere packing while the volume of the cubooctahedral voids is diminished. The anions of the VF_3-type compounds are in this model considered as hard spheres and the trivalent cations are located in the octahedral voids. The A-cation site is vacant in the VF_3-type structure and the simplest conceivable compression mechanism of compounds belonging to this structure type is a coupled rotation of the MF_6 octahedra around the *c*-axis (hexagonal setting), which will shorten the length of the *a*-axis and diminish the volume of the cubooctahedral voids while leaving the length of the *c*-axis unchanged. The linear compressibility of the *a*-axis is expected to be high as the restoring force is because of the bending of the M–F–M bonds, and a 30° rotation around one of the body diagonals of the $Pm\bar{3}m$ structure leads to the hexagonal close packing of the framework atoms *X*. The ∠M–F–M bond angle decreases from 180° in the cubic $Pm\bar{3}m$ structure to 131.8° when hexagonal close packing of the F atoms is achieved.

Several studies of the compression mechanism of VF_3-type compounds have been performed using both X-ray and neutron diffraction techniques. TiF_3 and FeF_3 were studied by high-pressure X-ray diffraction and both compounds were found to exhibit pressure-induced octahedral strain at elevated pressures. The compression mechanism was found to be anisotropic as the volume reduction was achieved through shortening of the hexagonal *a* lattice parameter, while *c*-lattice parameter was found to exhibit a small elongation for increasing pressures (Sowa and Ahsbahs, 1998). In addition, CrF_3 and FeF_3 have been studied by time-of-flight neutron powder diffraction and these studies showed that the ∠Cr–F–Cr bond angle was reduced from 144.80(7)° to 133.9(4)° at $p_{max} = 8.56$ GPa, while the corresponding ∠Fe–F–Fe bond angle was reduced from 152.5(2)° to 134.8(3)° at $p_{max} = 8.28$ GPa and both compounds were observed to develop pressure-induced octahedral strain (Jørgensen *et al.*, 2004, Jørgensen and Smith, 2006). The aim of the present experiment was to obtain detailed structural information on GaF_3 at elevated pressures.

[a]Author to whom correspondence should be addressed. Electronic mail: jenserik@chem.au.dk

II. EXPERIMENTAL

High-pressure X-ray diffractograms were measured on a powdered GaF_3 sample (Aldrich) loaded in a diamond anvil cell with methanol/ethanol (4:1) mixture as a pressure-transmitting medium. The sample was loaded into a hole of 200 μm in diameter drilled in a stainless steel gasket preindented to 70 μm. The measurements were performed at the Swiss-Norwegian Beam Lines (BM1A) of the European Synchrotron Radiation Facility (ESRF, Grenoble, France) using a wavelength of 0.69775 Å and MAR345 image plate detector. The wavelength, sample-to-detector distance (250 mm) and parameters of the detector were calibrated using NIST standard LaB_6. The beam was slit collimated to 100 × 100 μm^2. Pressure was determined on a ruby crystal with ~0.1 GPa precision (Forman *et al.*, 1972; Mao *et al.*, 1986). The recorded powder patterns were first integrated in the FIT2D software and then analysed by the Rietveld method using the FullProf program suite (Rodríguez-Carvajal, 1993). CrystalExplorer (Version 3.1) was used for illustrating void spaces (Wolff *et al.*, 2012).

III. RESULTS AND DISCUSSION

Powder diffraction profiles of GaF_3 were recorded in the pressure range from 0.0001 to 10 GPa and inspection of the peak profiles gave no indication of any change of symmetry. Rietveld refinements of the measured powder diffraction profiles were therefore performed in space group $R\bar{3}c$. Small Bragg peaks originating from a minor impurity of $GaF_3.3H_2O$ were visible in powder patterns recorded for $p \leq 3$ GPa. The $GaF_3.3H_2O$ phase was included in the Rietveld refinements for $p \leq 3$ GPa using structural parameters from the isostructural fluoro-hydrate $CrF_3.3H_2O$ (Herbstein *et al.*, 1985). The refined structural parameters of GaF_3 are given in Table 1 and Figure 1 shows, as a representative example, the measured and calculated X-ray powder diffraction profiles of GaF_3 at 10 GPa. The pressure dependence of the lattice parameters a and c (hexagonal setting) is shown in Figure 2. The a-axis decreases monotonically with the pressure and it is reduced by 8.8% at the highest measured pressure of 10 GPa and a change in the linear compressibility is observed at ≈4 GPa. The pressure dependence of the c-axis is much smaller and non-monotonous as it exhibits a maximum at ≈3 GPa (0.17% increase), while the overall reduction is 0.4% at 10 GPa. The insert of Figure 2 shows the $\sqrt{3}/3 \cdot c/a$ ratio vs. pressure. This ratio is equal to 1.633 at ≈7.9 GPa corresponding to hexagonal close packing of the fluorine atoms. The volume of the unit cell is plotted as a function of pressure in Figure 3 and a change in the compressibility is again observed at ≈4 GPa where the compressibility is seen to decrease. The unit-cell volume is reduced by 10.6% at 4 GPa and the reduction increases to 17.2% at 10 GPa. The data measured for $p \leq 4$ GPa were used for the determination of the bulk modulus B_0 of GaF_3 by use of the third-order Birch–Murnaghan equation of state:

$$P = \frac{3}{2} \cdot B_0 (x^{-7/3} - x^{-5/3}) \left[1 - \frac{3}{4} \cdot (4 - B'_0)(x^{-2/3} - 1) \right], \quad (1)$$

where x denotes the volume ratio V/V_0 (with V_0 being the volume at zero pressure) while B_0 and B'_0 are the isothermal bulk modulus at ambient pressure and its pressure derivative, respectively. The least-squares fit to the measured data yielded the following value for the bulk modulus: $B_0 = 28(1)$ GPa with B'_0 and fixed at the values of 4 and $V_0 = 282(2)$ $Å^3$.

TABLE I. Refined structural parameters for GaF_3.

p (GPa)	a (Å)	c (Å)	x	R_{Bragg} (%)	R_F (%)
0.0001	4.9818(3)	13.016(1)	0.5995(7)	4.34	3.50
1.0	4.9244(4)	13.018(1)	0.6069(8)	4.62	3.18
2.0	4.8553(4)	13.030(1)	0.6151(8)	4.39	2.98
3.0	4.7851(5)	13.039(1)	0.6181(9)	7.13	4.81
4.0	4.7077(4)	13.032(1)	0.632(1)	5.22	4.02
5.0	4.6736(4)	13.015(1)	0.6350(9)	4.01	3.64
6.0	4.6426(4)	12.999(1)	0.6379(9)	4.08	3.99
7.0	4.6186(4)	12.997(1)	0.6430(8)	3.35	2.80
8.0	4.5890(6)	12.988(2)	0.6485(9)	4.02	2.95
9.0	4.5670(8)	12.977(2)	0.651(1)	...4.72	3.41
10.0	4.5435(8)	12.958(3)	0.655(1)	5.45	3.68

Space group: $R\bar{3}c$ #167, Ga: 6b (0 0 0), F: 18e (x 0 ¼).

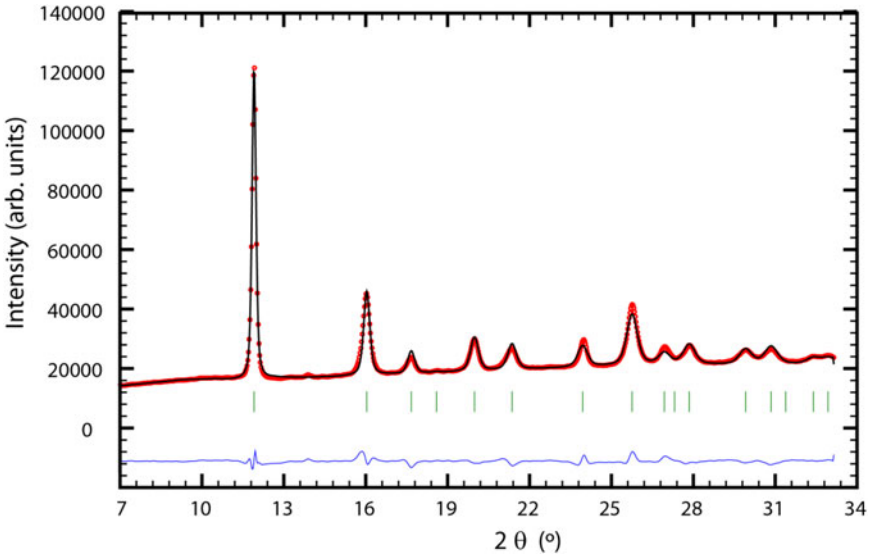

Figure 1. (Color online) Observed (red dots) and calculated (black curve) X-ray powder diffraction profiles of GaF_3 at 10 GPa. Green vertical bars mark the positions of the Bragg reflections and the lower blue curve represents the difference between the observed and calculated intensities.

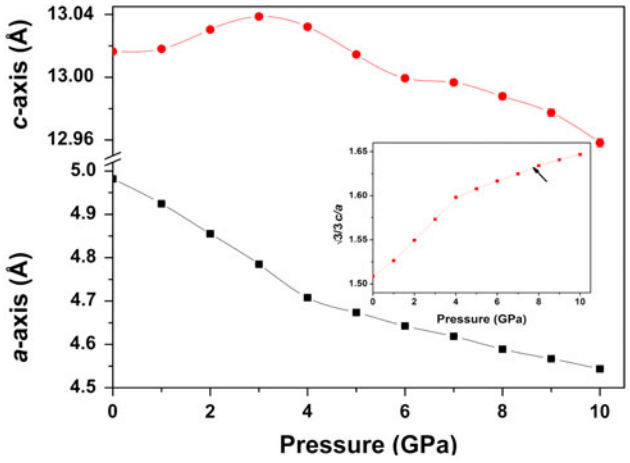

Figure 2. (Color online) Lattice parameters a and c plotted as a function of pressure. The a- and c-axes are reduced by 8.8 and 0.4%, respectively, at 10 GPa and the c-axis expands slightly up to ≈3 GPa. An anomalous change in compressibility is observed at ≈4 GPa. The insert shows the $\sqrt{3}/3 \cdot c/a$ ratio vs. pressure. This ratio is equal to 1.633 at ≈7.9 GPa corresponding to hexagonal close packing of the fluorine atoms.

The simplest description of the compression mechanism of VF_3-type compounds is in terms of deformation of an 8/3/c2 sphere-packing model in space group $R\bar{3}c$ as mentioned above and the x-coordinate of the spheres (F atoms) is in this model determined by c/a ratio and given by Sowa and Ahsbahs (1998):

$$x = \frac{1}{2} \pm \left[\frac{c^2}{72a^2} - \left(\frac{1}{12}\right)\right]^{1/2}. \quad (2)$$

Figure 4 shows the c/a ratio plotted as function of the fluorine x-coordinates. The deformation of the 8/3/c2 sphere-packing model gives a reasonable description of the compression mechanism of GaF_3 as the observed linear compressibility the a-axis is substantially larger than that of the c-axis. However, minor but significant deviations from the sphere-packing model are observed and the refined c/a and x-values

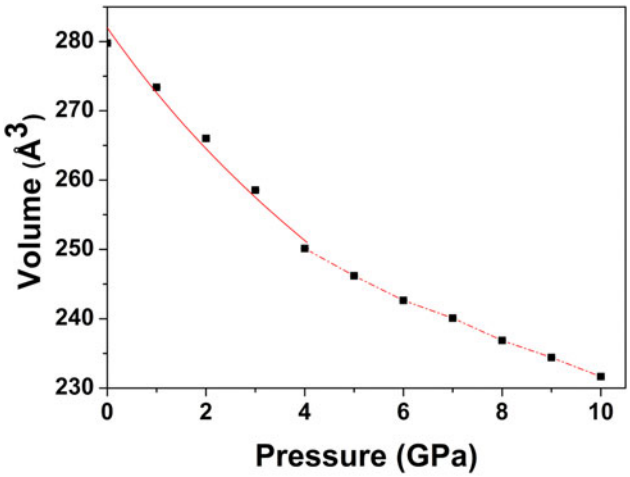

Figure 3. (Color online) Unit-cell volume of GaF_3 plotted as a function of pressure. The solid red line represents a fit to third-order Birch–Murnaghan equation of state yielding bulk modulus $B_0 = 28(1)$ GPa (see text). The dash-dotted line is a guide to the eye.

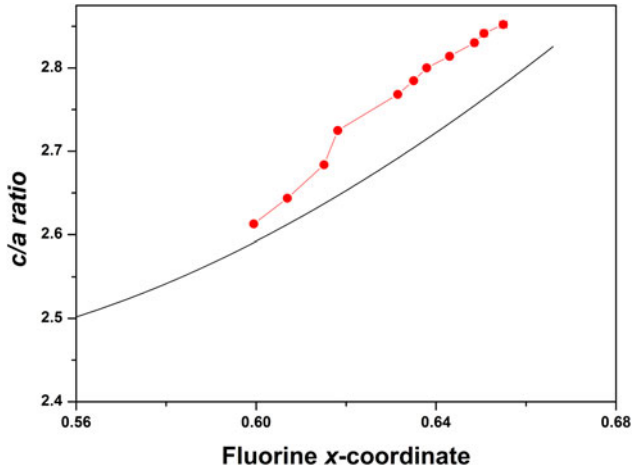

Figure 4. (Color online) The c/a ratio plotted as function of the refined fluorine x-coordinates. The solid line is calculated from the 8/3/c2 sphere-packing model (see text). An increasing deviation from the sphere packing model is observed for increasing values of x (corresponding to increasing pressure).

for GaF_3 show an increasing deviation from the sphere packing model at elevated pressures and the non-monotonous pressure dependence of the length of the c-axis is also at variance with the predictions of the 8/3/c2 sphere-packing model, which predicts a constant length of this axis during compression.

The pressure-induced structural changes of the GaF_6 octahedra are depicted in Figures 5 and 6. The Ga–F bond length and the two independent F–F distances d_1 and d_2 within the GaF_6 octahedra are plotted as function of pressure in Figure 5, which shows that the Ga–F bond length is reduced by 0.8% at 10 GPa, while the F–F distances d_1 and d_2 decrease monotonically by 2.1 and 1.0%, respectively, up to ≈4 GPa and become constant above this pressure. Figure 6 shows the volume of the GaF_6 octahedra and the octahedral strain

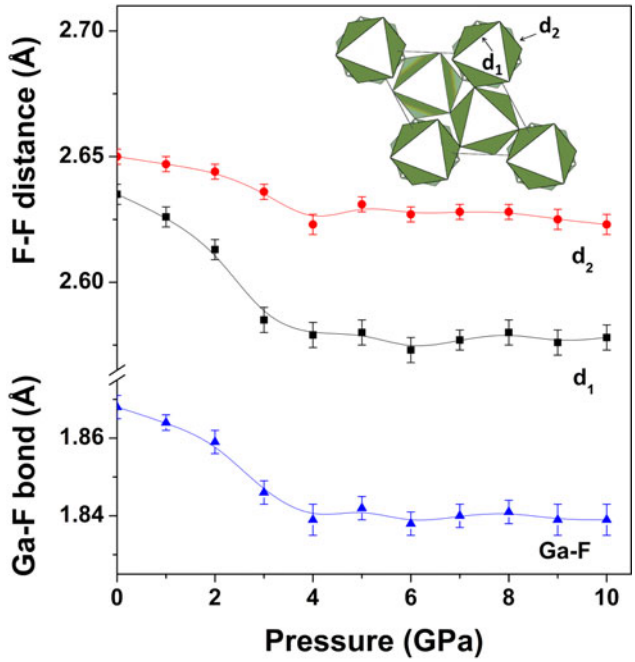

Figure 5. (Color online) Ga–F bond length and intra octahedral F–F distances d_1 and d_2 plotted as a function of pressure. The intra-octahedral F–F distances d_1 and d_2 are defined in the insert, which shows the GaF_3 structure at ambient pressure viewed along the c-axis.

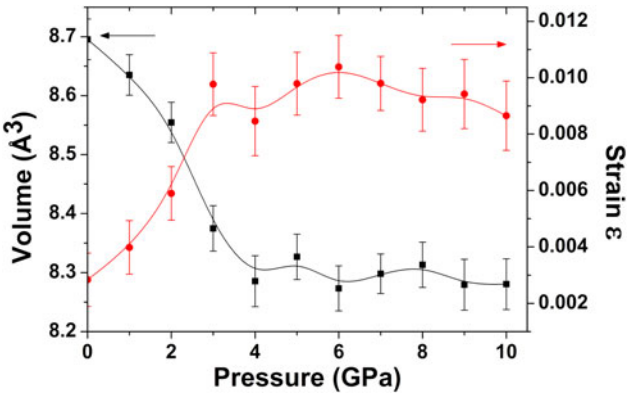

Figure 6. (Color online) Volume of the GaF_6 octahedra and octahedral strain $\varepsilon = |d_1 - d_2|/(d_1 + d_2)$ plotted as a function of pressure.

$[\varepsilon = |d_1 - d_2|/(d_1 + d_2)]$ plotted as a function of pressure. The volume of the GaF_6 octahedra is reduced by 4.6% at ≈4 GPa and stays constant above this pressure. The octahedral strain ε initially also increases and saturates at a constant value for pressures higher than ≈3 GPa. The initial volume reduction of 4.6% of the GaF_6 octahedra therefore accounts for ≈43% of the total volume reduction at 4 GPa and the increasing degree of distortion reflects an increasing elongation of the GaF_6 octahedra along the c-axis ($d_1 < d_2$). The elongation of the GaF_6 octahedra also explains the fact that the $\sqrt{3}/3 \cdot c/a$ ratio exceeds 1.633 for $p \gtrsim 7.9$ GPa as shown in the insert of Figure 2. The above-mentioned coupled rotation angle ω of the GaF_6 octahedra around the c-axis is calculated from the refined fluorine x-coordinates. A calculation of ω shows that it increases from 19.0(1)° at ambient pressure to 24.5(2)° at 4 GPa, and it is therefore concluded that compression of GaF_3 is achieved through reduction of the volume of the GaF_6 octahedra as well as through reduction of the volume of the cubooctahedral voids for $p \leq 4$ GPa. The observed constant values of volume and strain of the GaF_6 octahedra for $p \geq 4$ GPa show that they become almost rigid polyhedra at elevated pressures. Compression of GaF_3 is therefore almost entirely achieved through reduction of the volume of the cubooctahedral voids in this pressure range where ω increases to 28.2(2)° at 10 GPa, showing that the fluorine atoms are almost hexagonally close packed at this pressure. The corresponding ∠Ga–F–Ga bond angle was found to decrease from 145.01(5)° to 135.00(8)° within the pressure range from 0.0001 to 10 GPa and thereby approaching the value of 131.8° predicted by the 8/3/c2 sphere-packing model in the limit of hexagonally close packed spheres.

The reduction of the volume of the cubooctahedral voids is visualized in Figure 7, which shows the crystal structures of GaF_3 and the cubooctahedral voids at ambient pressure, 5 and 10 GPa. The cubooctahedral voids are visualized as isosurfaces of the procrystal electron density (Turner *et al.*, 2011). The three isosurfaces are drawn for isovalues of 0.005 $e(Å^{-3})$ and cubooctahedral voids are seen to shrink for increasing pressures as predicted by the 8/3/c2 sphere-packing model. The volume of the cubooctahedral voids is reduced by 79% at 5 GPa and almost absent (99% reduction) at 10 GPa consistent with the proximity to close packing of the F^- ions at this pressure as described above.

A comparison of the high-pressure behaviour TiF_3, CrF_3, FeF_3, and GaF_3 shows that their compression mechanisms are very similar although with minor differences. The c-axis of all four compounds exhibits negative linear compressibility at lower pressures and the octahedral strain ε increases at elevated pressures for all four compounds. The c-axis of TiF_3 is elongated by 2.9% between 0.0001 and 5 GPa (Sowa and Ahsbahs, 1998), which is substantially larger than the corresponding values of 0.17% observed for GaF_3 and CrF_3 (Jørgensen *et al.*, 2004). In the case of FeF_3 intermediate elongations of 0.77 and 1.1% of the c-axis have been observed (Sowa and Ahsbahs, 1998; Jørgensen and Smith, 2006). The octahedral stain ε of GaF_3 saturates at ≈0.009 for $p \gtrsim 3$ GPa, which is comparable with the corresponding ε values of 0.005 and 0.008 for CrF_3 and FeF_3, respectively (Jørgensen *et al.*, 2004, Jørgensen and Smith, 2006). In addition, analysis of the results of Sowa and Ahsbahs (1998) for TiF_3 and FeF_3 shows that the octahedral strain ε increases linearly up to about 3 GPa and saturates at values of 0.014 and 0.0063 for TiF_3 and FeF_3, respectively. However, in contrast to the high-pressure neutron diffraction studies of CrF_3 and FeF_3 (Jørgensen *et al.*, 2004, Jørgensen and Smith, 2006), no structural refinement was done in this study (Sowa and Ahsbahs, 1998), which was based on the assumption that the metal–fluorine bond length is independent of the pressure. Most interestingly, the observed change in the compressibility of GaF_3 at ≈4 GPa as well as the initial reduction of volume of the GaF_6 octahedra seems to be unique to this compound. The change in compressibility and the initial reduction of the volume of the GaF_6 octahedra is mainly because of changes in the

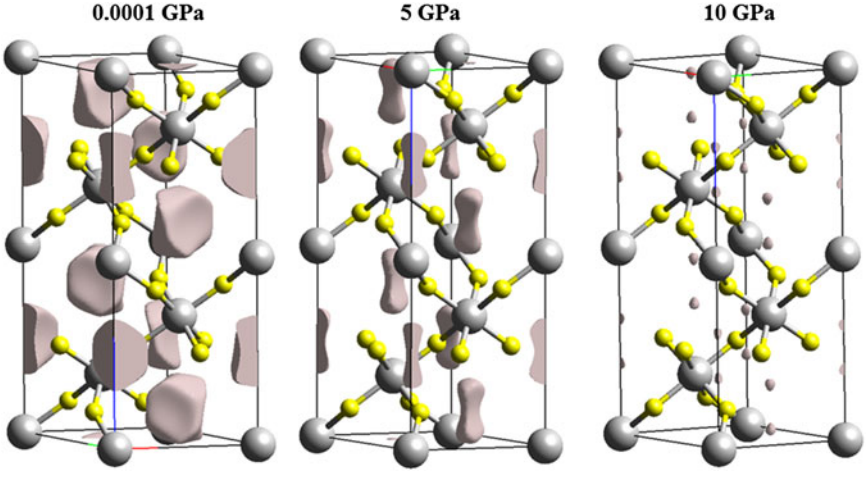

Figure 7. (Color online) Crystal structure of GaF_3, including cubooctahedral voids at 0.0001, 5, and 10 GPa. Small yellow spheres and large grey spheres represent Ga and F, respectively. The isosurfaces of the cubooctahedral voids are drawn for isovalues of 0.005 $e(Å^{-3})$. The volume of cubooctahedral voids are reduced by 79 and 99% at 5 and 10 GPa, respectively.

Ga–F bond length and d_1 F–F distance. The Ga–F bond length and d_1 F–F distance decreases up to about 4 GPa and becomes constant above this pressure and similar behaviour is not observed in the earlier high-pressure studies of CrF_3 and FeF_3 (Jørgensen *et al.*, 2004, Jørgensen and Smith, 2006).

IV. CONCLUSION

The compression mechanism of GaF_3 was found to be highly anisotropic with the lengths of *a*- and *c*-axes being reduced by 8.8 and 0.4%, respectively, at the highest measured pressure of 10 GPa. The initial compression up to about 4 GPa is achieved through coupled rotations of the GaF_6 octahedra around the *c*-axis, which is accompanied by volume reduction and distortion of the GaF_6 octahedra, which become rigid polyhedral for pressures higher than 4 GPa. Compression at higher pressures is entirely achieved through the coupled rotation of the GaF_6 octahedra which reduces the volume of the cubooctahedral voids. In addition, our work shows the usefulness of isosurfaces of the procrystal electron density for illustrating changes in void space in crystals at elevated pressures.

ACKNOWLEDGEMENT

The corresponding author JEJ gratefully acknowledge the beam time granted on at the Swiss-Norwegian Beam Lines (BM1A) at the European Synchrotron Radiation Facility (ESRF, Grenoble, France).

Fischer, W. (**1973**). "Existenzbedingungen homogener Kugelpackungen zu kubischen Gitterkomplexen mit weniger als drei Freiheitsgraden," Z. Kristallogr. **138**, 129–146.

Forman, R. A., Piermarini, G. J., Barnett, J. D., and Block, S. (**1972**). "Pressure measurement made by the utilization of ruby sharp-line luminescence," Science **176**, 284–285.

Herbstein, F. H., Kapon, M., and Reisner, G. M. (**1985**). "Crystal structures of chromium(III) fluoride trihydrate and chromium(III) fluoride pentahydrate. Structural chemistry of hydrated transition metal fluorides. Thermal decomposition of chromium(III) fluoride nonahydrate," Z. Kristallogr. **171**, 209–224.

Jørgensen, J.-E. and Smith, R. I. (**2006**). "On the compression mechanism of FeF_3," Acta Crystallogr. B **62**, 987–992.

Jørgensen, J.-E., Marshall, W. G., and Smith, R. I. (**2004**). "The compression mechanism of CrF_3," Acta Crystallogr. B **60**, 669–673.

Leblanc, M., Pannetier, J., Ferey, G., and de Pape, R. (**1985**). "Single-crystal refinement of the structure of rhombohedral FeF_3," Rev. Chim. Miner. **22**, 107–114.

Mao, H. K., Xu, J., and Bell, P. M. (**1986**). "Calibration of the ruby pressure gauge to 800-kbar under quasi-hydrostatic conditions," J. Geophys. Res. Solid Earth Planets **91**, 4673–4676.

Meisel, K. (**1932**). "Rheniumtrioxyd III. Mitteilung: Über die Kristallstruktur des Rheniumtrioxyds," Z. Anorg. Allgem. Chem. **207**, 121–128.

Rodríguez-Carvajal, J. (**1993**). "Recent advances in magnetic structure determination by neutron powder diffraction," Physica B **192**, 55–69.

Roos, M. and Meyer, G. (**2001**). "Refinement of the crystal structure of gallium trifluoride, GaF_3," Z. Kristallogr. New Cryst. Struct. **216**, 18.

Sowa, H. and Ahsbahs, H. (**1998**). "Pressure-induced octahedron strain in VF_3-type compounds," Acta Crystallogr. B **54**, 578–584.

Turner, M. J., McKinnon, J. J., Dylan Jayatilaka, D., and Spackman, M. A. (**2011**). "Visualisation and characterisation of voids in crystalline materials," CrystEngComm **13**, 1804–1813.

Wolff, S. K., Grimwood, D. J., McKinnon, J. J., Jayatilaka, D., and Spackman, M. A. (**2012**). *CrystalExplorer* (*Version 3.1*) (University of Western Australia).